Energy fluctuations in spin glasses

Helmut G. Katzgraber,[1] Mathias Körner,[1] Frauke Liers,[2] Michael Jünger,[2] and A. K. Hartmann[3]

[1] *Theoretische Physik, ETH Hönggerberg, CH-8093 Zürich, Switzerland*
[2] *Universität zu Köln, Institut für Informatik, Pohligstrasse 1, 50969, Köln, Germany*
[3] *Institut für Theoretische Physik, Universität Göttingen, Friedrich-Hund-Platz 1, 37077 Göttingen, Germany*

(Dated: June 13, 2005)

We study the probability distribution function of the ground-state energies of the disordered one-dimensional Ising spin chain with power-law interactions using a combination of parallel tempering Monte Carlo and branch, cut & price algorithms. By tuning the exponent of the power-law interactions we are able to scan several universality classes. Our results suggest that mean-field models have a non-Gaussian limiting distribution of the ground-state energies, whereas non-mean-field models have a Gaussian limiting distribution. We compare the results of the disordered one-dimensional Ising chain to results for a disordered two-leg ladder, for which large system sizes can be studied, and find a qualitative agreement between the disordered one-dimensional Ising chain in the short-range universality class and the disordered two-leg ladder. We show that the mean and the standard deviation of the ground-state energy distributions are well described by a power-law behavior. In the mean-field universality class the skewness does not follow a power-law behavior and converges to a nonzero constant value. The data for the Sherrington-Kirkpatrick model seem to be acceptably well fitted by a modified Gumbel distribution. Finally, we discuss the distribution of the internal energy of the Sherrington-Kirkpatrick model at finite temperatures and show that it behaves similar to the ground-state energy of the system if the temperature is smaller than the critical temperature.

PACS numbers: 75.50.Lk, 75.40.Mg, 05.50.+q

I. INTRODUCTION

Averages of physical quantities and their fluctuations play an important role in statistical physics; however the knowledge of the "average" behavior of a quantity often does not provide sufficient information to fully characterize a system, especially if the probability distribution of the quantity in question is non-Gaussian, e.g., when it has a non-vanishing skewness or exhibits a "fat" tail.[1] Hallmark examples of such distributions are power-law or exponential distributions, which in nature occur in relation to earthquakes,[2] magnetic fluctuations,[3] stock markets,[4] directed polymer in a random medium,[5,6] coauthorships in publications, the Internet, and other complex networks.[7] Many of these systems are characterized by the absence of a characteristic length scale such that rare events involving large parts of the system become important and strongly influence the average of various quantities.

Recently, there has been a renewed interest the ground-state energy distribution $P(E)$ and its limiting form $P_\infty(E)$ of the mean-field Sherrington-Kirkpatrick (SK) spin-glass model[8,9] and of short-range spin glasses in two and three dimensions.[10] While studies of the mean-field model have found a non-Gaussian limiting distribution,[8,9] the study of small system sizes of two and three dimensional short-range spin glasses[10] have found a Gaussian limiting distribution in the thermodynamic limit. This is supported by the fact that systems with short-range interactions can be subdivided into smaller subsystems, coupled weakly enough to contribute almost independently to the total energy and leading to a Gaussian distribution via the central-limit theorem;[10] however it is important to note that the weak coupling between the ground-state energies of subsystems below or at an ordering temperature is not self-evident.

Our goal is to consolidate the different limiting cases of short-range and long-range interactions in spin glasses[11] by studying a disordered one-dimensional Ising spin chain with power-law interactions.[12–16] The model has the advantage over conventional models in that by tuning the power-law exponent, several universality classes ranging from mean-field type behavior to a short-range spin glass can be probed for a large range of system sizes. We show that the phase-space complexity — i.e., the presence or absence of *mean-field behavior*[17] — is reflected in the limiting distribution of the ground-state energies. We also study a two-leg short-range spin ladder, where an exact transfer-matrix algorithm can be applied, in order to compute relevant moments of the energy distributions for large system sizes and to obtain a comparison for the results of the disordered Ising chain with power-law interactions in the short-range phase. Using a large range of system sizes, our results clearly show that mean-field spin-glass models have a non-Gaussian limiting distribution with a finite skewness in the thermodynamic limit, whereas the limiting distributions for non-mean-field models are Gaussian (also referred to as "Normal"). In addition, we also find that the distribution of the internal energy of mean-field models is non-Gaussian if the temperature is lower than the critical temperature.

We do not attempt to make a prediction regarding the exact functional form of the limiting distribution for an arbitrary spin-glass model. Bouchaud *et al.*[10] have shown for small L that typical short-range spin glass

models have a Normal limiting distribution. This is not the case for the mean-field model, thus posing the question of whether the limiting distribution falls into one of the standard three universality classes for the minimum of uncorrelated variables:[1] Gumbel, Fischer-Tippet-Frèchet, and Weibull distributions. The results of Bouchaud *et al.*[10] cannot determine with certainty which limiting distribution fits the data best.[18] Our results suggest that a modified Gumbel distribution[3,8,19] fits the data for the SK model best, although a detailed probing of the tails of the energy distributions would be required to make a definite statement if corrections to the modified Gumbel distribution are required. For finite values of the power-law exponent we add a quadratic correction to the modified Gumbel distribution and show that for finite system sizes the data are well described by this function. In addition, the quadratic correction (Gaussian) dominates for increasing system size in the non-mean-field universality class, thus showing that in the thermodynamic limit a Normal distribution is recovered.

General scaling arguments are presented in Sec. II. In Sec. III we present results on a one-dimensional two-leg ladder with short-range interactions in order to illustrate the expected results for a short range model for very large system sizes. Results on the one-dimensional Ising spin chain with power-law interactions at zero and finite temperatures are presented in Sec. IV. We conclude in Sec. V. The numerical methods used to compute the ground-state energies[20,21] are described in the Appendix.

II. STATISTICAL DESCRIPTION OF DATA

In general, we expect the ground-state energy of a disordered system to be a random variable with mean $\langle E\rangle$, standard deviation σ_E, and skewness ζ_E.[22] In this work we study the size-dependence of the aforementioned observables. In particular, we surmise that the mean ground-state energy of a (one-dimensional) random system scales as

$$[\langle E\rangle - E_\infty]/L = aL^{-\omega} \; , \tag{1}$$

where L represents the system size (and number of spins) and ω describes the leading finite-size corrections for the energy per spin. We keep the extra factor of L in Eq. (1), as well as in the following definitions in order to be able to compare to the exponent estimates of Ref. 8. The standard deviation of the ground-state energy of a general disordered system can be expected to be determined by an exponent ρ via

$$\sigma_E/L = bL^{-\rho} \; . \tag{2}$$

The skewness of a distribution of M values $\{E_i\}$ is given by

$$\zeta_E = \frac{1}{M}\sum_{i=1}^{M}\left[\frac{E_i - \langle E\rangle}{\sigma_E}\right]^3 \; , \tag{3}$$

where $\langle E\rangle$ and σ_E are given by Eqs. (1) and (2), respectively. Note that the skewness is a dimensionless quantity. Following previous results by Ref. 10 we expect the skewness to decay as

$$\zeta_E = c_1 + c_2 L^{-\gamma} \tag{4}$$

with $\gamma > 0$. As we shall see later, $c_1 = 0$ for the short-range limit of the model. We also want to test whether the scaled probability distribution functions $P(\epsilon)$ with $\epsilon = (E - \langle E\rangle)/\sigma_E$ converge to a limiting form $P_\infty(\epsilon)$ for $L \to \infty$. If this is the case, then data for the ground-state energies should be scalable via

$$P(E) = \frac{1}{\sigma_E} P_\infty\left(\frac{E - \langle E\rangle}{\sigma_E}\right) \; , \tag{5}$$

where $\langle E\rangle$ and σ_E are given by Eqs. (1) and (2), respectively.

III. TWO-LEG SPIN-GLASS LADDER

To compare results for the one-dimensional Ising spin chain with power-law interactions with a simple benchmark model for which large system sizes can be studied, we consider a disordered (short-range) Ising model on a two-leg ladder (see Fig. 1). The couplings J_{ij} between nearest-neighbor spins are chosen from a Normal distribution with zero mean and unit standard deviation. A system of length L is described by the Hamiltonian

$$\begin{aligned}\mathcal{H} \; &= \; \sum_{l=1}^{L} J_{(l,a),(l,b)}\, S_{(l,a)}\, S_{(l,b)} \\ &+ \sum_{l=1}^{L-1}\sum_{i=a,b} J_{(l,i),(l+1,i)}\, S_{(l,i)}\, S_{(l+1,i)} . \end{aligned} \tag{6}$$

The first summation in Eq. (6) runs over all rungs l, while the second summation runs over all exchanges between the rungs, and $S_{(l,i)} = \pm 1$ is the value of the (Ising) spin on the i-th leg of the l-th rung of the ladder. The ground-state energy of the system can be efficiently calculated with a transfer-matrix algorithm.[23,24] The transfer-matrix algorithm computes the ground-state energy of a system of size L in $O(L)$ time so that large systems can be studied. The disorder average has to be performed explicitly by repeating the algorithm for a number of disorder realizations.

A. Numerical Method: Transfer Matrices

We can explain the transfer matrix algorithm by starting with a ladder of length L and assuming that the ground-state energy $E_{\rm g}(L, \{S_{(L,i)}\})$ of the ladder is known as a function of the spin configuration $\{S_{(L,i)}\}$ of

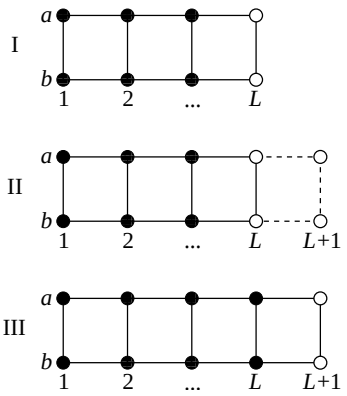

FIG. 1: Illustration of a step in the transfer-matrix calculation. Starting with a system of size L (panel I) whose ground-state energy is known as a function of the spins (open circles), we add another rung and calculate the change in energy $\Delta_{\rm E}$ given by the dashed line [see panel II and Eq. (8)]. The ground-state energy of the system as a function of the spins in the $L+1$-th rung is then calculated by taking the minimum of $E_{\rm g}+\Delta_{\rm E}$ over all configurations of the L-th rung [see panel III and Eq. (7)].

the L-th rung. We add the spins of the $L+1$-th rung to the system as illustrated in Fig. 1 and use the relation

$$E_{\rm g}(L+1,\{S_{(L+1,i)}\}) = \min_{\{S_{(L,i)}\}}\left[E_{\rm g}(L,\{S_{(L,i)}\}) + \Delta_{\rm E}(\{S_{(L,i)}\},\{S_{(L+1,i)}\})\right] \quad (7)$$

to integrate out the spins of the L-th rung and to obtain $E_{\rm g}$ as a function of the spins of the $L+1$-th rung. Here

$$\Delta_{\rm E}(\{S_{(L,i)}\},\{S_{(L+1,i)}\}) = \sum_{i=a,b} J_{(L,i),(L+1,i)}\, S_{(L,i)}\, S_{(L+1,i)} + J_{(L+1,a),(L+1,b)}\; S_{(L+1,a)}\, S_{(L+1,b)} \quad (8)$$

is the exchange energy of the spins added on the $L+1$-th rung with themselves and with the spins of the L-th rung. Starting with two spins, we iterate this procedure until the system has the desired size $L_{\rm max}$. The final ground-state energy is then obtained by minimizing over the spins of the last rung

$$E_g(L_{\rm max}) = \min_{\{S_{(L_{\rm max},i)}\}}\left[E_{\rm g}(L_{\rm max},\{S_{(L_{\rm max},i)}\})\right] . \quad (9)$$

We repeat the calculation until a desired number of disorder realizations is obtained.

B. Results

In Fig. 2 we scale the data for the energy of the ladder system according to Eq. (5) for system sizes up to $L = 10^4$. For each system size we compute 10^6 samples. The data scale well, although deviations are present in the tails. In particular, for small L the distribution is clearly skewed. For the short-ranged ladder system we

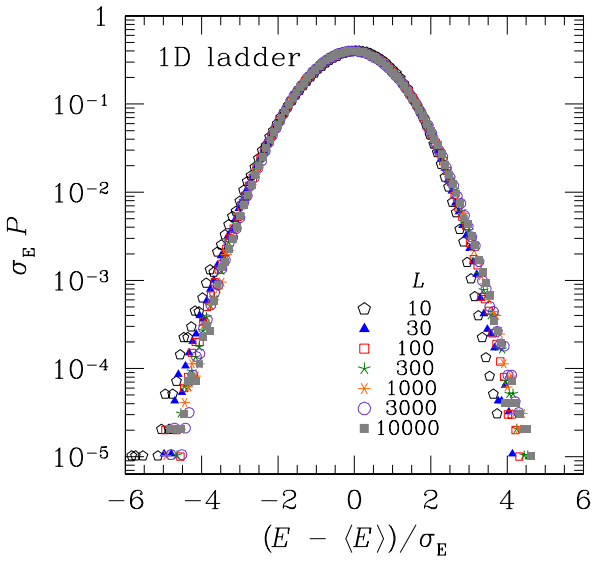

FIG. 2: (Color online) Scaling of the ground-state energy according to Eq. (5) for the ladder system. The data scale well, although deviations in the tails suggest that the skewness of the function is changing with system size L.

obtain a clear power-law decay of the skewness according to Eq. (4) with $\gamma \approx 0.5$ (and $c_1 = 0$), as can be seen in Fig. 3. This suggests that in the thermodynamic limit the ground-state energies are Gaussian distributed. For completeness, we quote the results for the size-dependence of the mean and standard deviation. We obtain for the mean energy

$$\langle E\rangle = -2.12582(8) - 0.801(8)L^{0.996(4)} \quad (10)$$

and thus $\omega \approx 0$. For the fluctuations

$$\sigma_E = 0.976(5)L^{0.497(8)} . \quad (11)$$

Our results therefore show that $\rho \sim -1/2$ and $[\langle E\rangle - E_\infty] \sim 1/L$, a results that agrees with data on the one-dimensional Ising chain in the short-range universality class, see below.

The scaling of the skewness to zero with a power law and the results for very large system sizes already suggest that for short-ranged systems the limiting distribution of the ground-state energy is Normal. This result differs from recent results[8] for the mean-field Sherrington-Kirkpatrick model,[25] where the limiting distribution P_∞ seems to have a finite skewness and thus cannot be properly described by a Gaussian. Hence, it is desirable to study a system that allows to interpolate between both cases. Thus one can verify whether the change of the distribution coincides with a general change of the phase-space structure. This is indeed the case for the one-dimensional long-range Ising spin glass, which is studied in the following section.

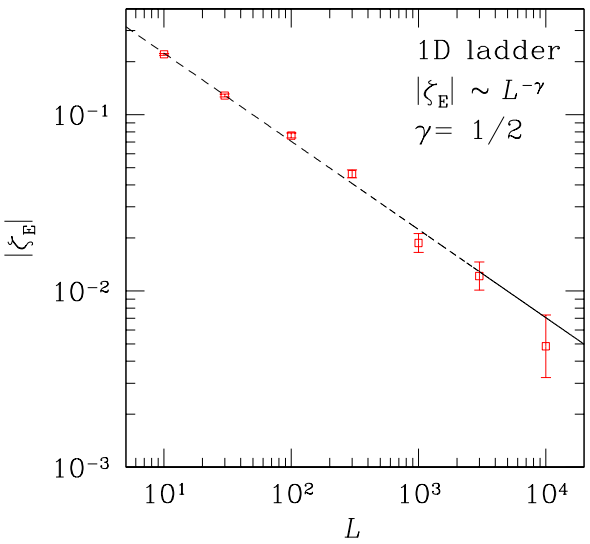

FIG. 3: (Color online) Skewness of the energy distributions as a function of system size L for the ladder system. The skewness can be well fitted to a power-law decay with an exponent $\gamma \sim 1/2$. This suggests that in the thermodynamic limit the limiting distribution is Gaussian (zero skewness).

IV. 1D ISING CHAIN

The Hamiltonian for the one-dimensional long-range Ising spin glass with power-law interactions is given by

$$\mathcal{H} = -\sum_{i,j} J_{ij} S_i S_j \ , \tag{12}$$

where $S_i = \pm 1$ represent Ising spins evenly distributed on a ring of length L in order to ensure periodic boundary conditions. The sum is over all spins on the chain and the couplings J_{ij} are given by[15]

$$J_{ij} = c(\sigma)\frac{\epsilon_{ij}}{r_{ij}^{\sigma}} \ , \tag{13}$$

where the ϵ_{ij} are chosen according to a Gaussian distribution with zero mean and standard deviation unity:

$$\mathcal{P}(\epsilon_{ij}) = \frac{1}{\sqrt{2\pi}} \exp(-\epsilon_{ij}^2/2) \tag{14}$$

and $r_{ij} = (L/\pi)\sin[(\pi|i-j|)/L]$ represents the *geometric* distance between the spins on the ring.[26] The power-law exponent σ determines the range of the interactions and thus the universality class of the model, as described in the next section. The constant $c(\sigma)$ in Eq. (13) is chosen to give a mean-field transition temperature $T_c^{\rm MF} = 1$, where

$$\left(T_c^{\rm MF}\right)^2 = \sum_{j\neq i} [J_{ij}^2]_{\rm av} = c(\sigma)^2 \sum_{j\neq i} \frac{1}{r_{ij}^{2\sigma}} \ . \tag{15}$$

Here $[\cdots]_{\rm av}$ denotes an average over disorder. In this work we compute unscaled energies for the one-dimensional Ising chain. Thus we find the optimal configuration of spins $\{S_i\}$ that minimizes the Hamiltonian in Eq. (12) for a given set of interactions $\{J_{ij}\}$, i.e.,

$$E = \min_{\{S_i\}} \mathcal{H}(\{J_{ij}\},\{S_i\}) \, . \tag{16}$$

The (commonly used) energy per degree of freedom e is then given by $e = E/L$.

A. Phase Diagram

The d-dimensional long-range Ising spin glass with power-law interactions has a very rich phase diagram in the d-σ plane. This is summarized in Fig. 4, which is based on work performed by Bray *et al.*[12] and by Fisher and Huse[13] who present a detailed analysis of the role of long-range interactions within the droplet model. Spin-glass behavior is controlled by the long-range part of the interaction if σ is sufficiently small, and by the short-range part if σ is sufficiently large. More precisely, one has long-range behavior if the stiffness exponent[27] of the long-range (LR) universality class, $\theta_{\rm LR}$, is greater than that of the short-range (SR) universality class, $\theta_{\rm SR}$, and vice versa. In addition, there is an exact result for $\theta_{\rm LR}$, namely[12,13]

$$\theta_{\rm LR} = d - \sigma, \tag{17}$$

so long-range behavior occurs if

$$\sigma < \sigma_c(d) = d - \theta_{\rm SR}(d) \ . \tag{18}$$

Equation (17) indicates that critical exponents depend continuously on σ in the long-range region, even though they are independent of σ in the region controlled by the short-range part of the interaction. Thus we expect to be able to tune the different universality classes by changing the exponent σ. The condition for a finite-temperature transition is $\theta > 0$, where θ refers here to the greater of $\theta_{\rm SR}$ and $\theta_{\rm LR}$. For the short-range model, there is a finite-temperature transition (i.e., $\theta_{\rm SR} > 0$) for d larger than the lower critical dimension d_l, which is found numerically to lie between 2 and 3.[28–34] For $d = 1$, as in the present study, we obtain a finite transition temperature for $\sigma < 1$. For $\sigma < d/2$, the model would not have a thermodynamic limit (T_c would diverge) if the interactions were not scaled as shown in Eq. (15). The scaling leads to a power-law dependence on L with a negative exponent, i.e., $c(\sigma) \to 0$ for $L \to \infty$. $\sigma = 0$ corresponds to the SK model and leads to $c(0) \sim 1/L$.

B. Numerical Methods

Ground-state energies for the one-dimensional Ising chain are computed using the parallel tempering Monte

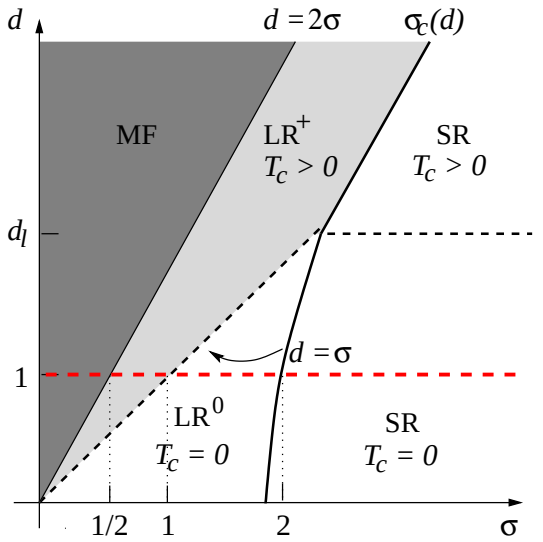

FIG. 4: (Color online) Sketch of the phase diagram in the d-σ plane for the spin-glass state of the disordered long-range Ising model with power-law interactions following Ref. 13. The light shaded region (LR^+) is where there is both a finite T_c and the spin-glass state is controlled by the long-range part of the interaction. The thick solid line separates the region of short-range behavior (SR) from that of long-range behavior and is denoted by $\sigma_c(d)$. The thick dashed line separates regions where $T_c = 0$ (e.g., LR^0) from regions where $T_c > 0$, i.e., it corresponds to a zero stiffness exponent. The dark shaded region (MF, $\sigma < d/2$) is where there is no thermodynamic limit unless the interactions are scaled appropriately by the system size. The calculations are performed for $d = 1$ (marked by a horizontal dashed red line), for which $\sigma_c(d) = 2$ within a droplet picture approximation. The thermodynamic limit does not exist for $\sigma < 1/2$ unless the interactions are scaled by a power of the system size. For $\sigma > 1$ $T_c = 0$. These values of σ are marked. (Figure adapted from Ref. 15).

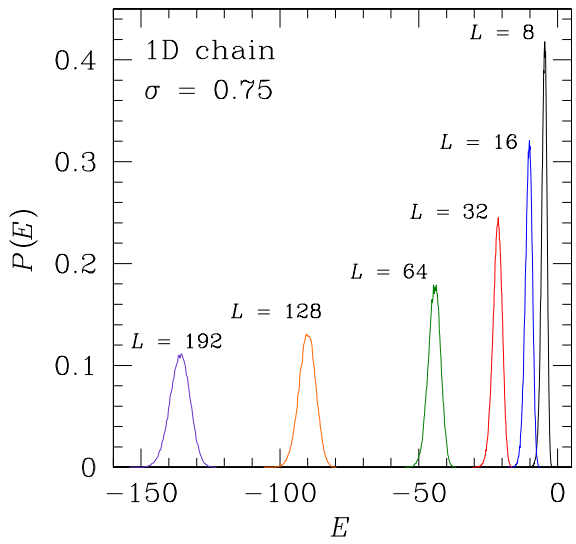

FIG. 5: (Color online) Unscaled energy distributions for several system sizes for the one-dimensional Ising chain with $\sigma = 0.75$ (LR^+ phase).

Carlo method[15,35–37] when the power-law exponent σ is small, and the branch, cut & price (BCP) algorithm[38–40] when σ is large. As reported in Ref. 16, the time to compute a ground-state instance using the parallel tempering Monte Carlo method scales in practice with a power of the system size for $\sigma \lesssim 1.25$, whereas for large values of σ the time to compute a ground state scales $\sim \exp(aL)$, with a a constant. In this case we use the BCP algorithm which performs best for short-range interactions, thus ideally complementing the parallel tempering method. Details about the algorithms used and simulation parameters can be found in the Appendix.

C. Results

For each system size we compute 10^5 ground-state realizations for system sizes up to $L = 192$ (see Table I for details). In Fig. 5 we show a representative set of the unscaled data for $\sigma = 0.75$ in the LR^+-phase for several system sizes. Data for other values of σ show a similar qualitative behavior. The data in Fig. 5 can be scaled according to Eq. (5), the result is displayed in Fig. 6. The data are clearly skewed and the tails indicate that the skewness depends on the system size. In Fig. 7 we show scaled data for the ground-state energy distributions for $\sigma = 0$ (SK limit, MF phase). The data also show a clear asymmetry, but the spread in the tails is noticeably smaller than for larger values of σ (see Figs. 6 and 8) suggesting a smaller dependence of the skewness of the distribution on the system size.

In order to better quantify the aforementioned behavior, in Fig. 9 we present data for the skewness as a function of system size for several values of the power-law exponent σ. The data show that for $\sigma > 0.5$ the skewness of the ground-state energy distributions decays with a power law $|\zeta_E| \sim L^{-\gamma}$, with $\gamma \approx 0.5$ in the SR phase, whereas for $\sigma \leq 0.5$ (MF phase) the skewness is well fitted by Eq. (4) with $c_1 > 0$ thus tending to a constant in the thermodynamic limit. This means that the mean-field models present a singular behavior in which the ground-state energy fluctuations are non-Gaussian in the thermodynamic limit. This is not the case for the non-mean-field universality class where a limiting Gaussian behavior is obtained for $L \to \infty$. Note that $\gamma \approx 0.5$ for $\sigma > 1$ for which $T_c = 0$, in agreement with the results for the ladder system studied in Sec. III.

We also study the size-dependence of the mean energy as a function of σ. For the mean-field Sherrington-Kirkpatrick model[25] ($\sigma = 0$) it is known that $\omega \sim 2/3$.[8–10,41] Our results agree well with this prediction, i.e., $\omega = 0.64(1)$ (the quality of fit probability[22] is $Q = 0.51$; the fit is performed for $L \geq 64$). Unfortunately, there are no predictions for the different exponents for $\sigma > 0$,

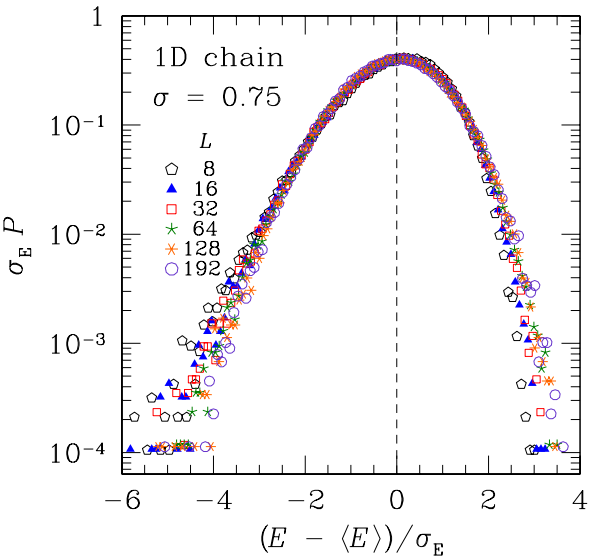

FIG. 6: (Color online) Scaled ground-state energy distributions for several system sizes for the one-dimensional Ising chain with $\sigma = 0.75$ (LR^{+} phase). The dashed vertical line is a guide to the eye to illustrate the skewness of the distribution. The spread of the data in the tails suggests that the skewness changes with system size.

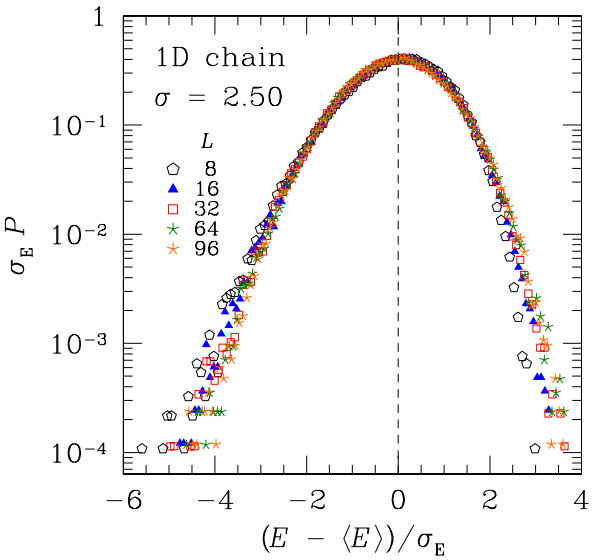

FIG. 8: (Color online) Scaled ground-state energy distributions for several system sizes for the one-dimensional Ising chain with $\sigma = 2.50$ (SR phase). The dashed vertical line is a guide to the eye to illustrate the skewness of the distribution. The data show a moderate dependence on the system size.

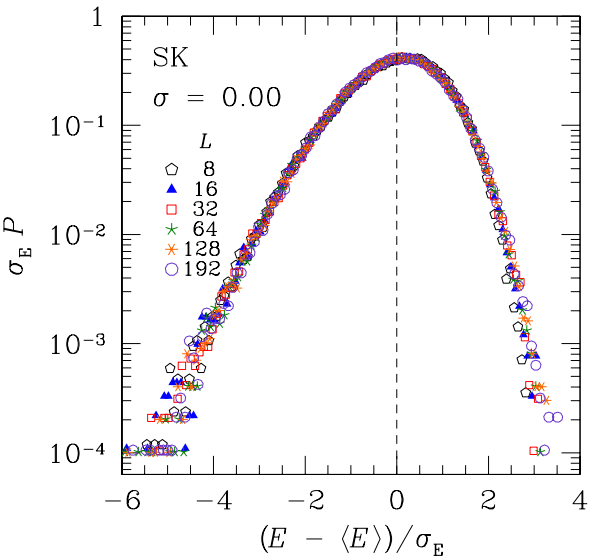

FIG. 7: (Color online) Scaled ground-state energy distributions for several system sizes for the one-dimensional Ising chain with $\sigma = 0$ (MF phase, SK model). The dashed vertical line is a guide to the eye to illustrate the skewness of the distribution. The data show little spread in the tails suggesting a weaker dependence on L than for larger values of σ.

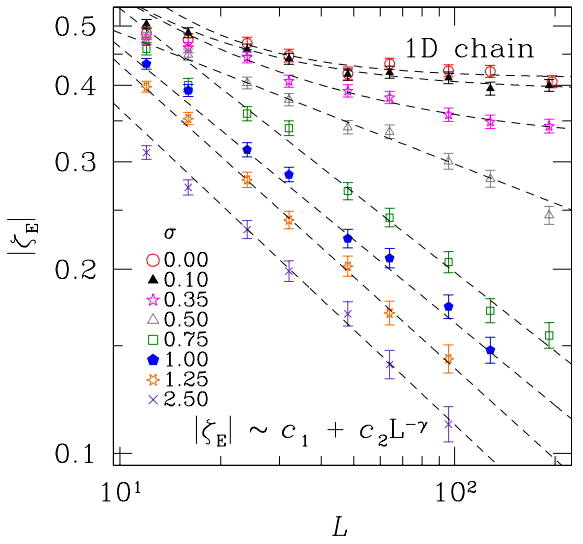

FIG. 9: (Color online) Skewness ζ_E as a function of system size L for several values of σ. For $\sigma < 0.5$ (MF phase) the data scale as $\zeta_E \sim c_1 + c_2 L^{-\gamma}$ with $c_1 > 0$ [Eq. (4)] thus tending to a constant in the thermodynamic limit. For $\sigma \geq 0.5$ the skewness decays with a power-law behavior, i.e., $c_1 = 0$ (fits done for $L \geq 64$). Note that for $\sigma > 1$, for which $T_c = 0$, $\gamma \approx 0.5$ in agreement with the results for the ladder system presented in Sec. III.

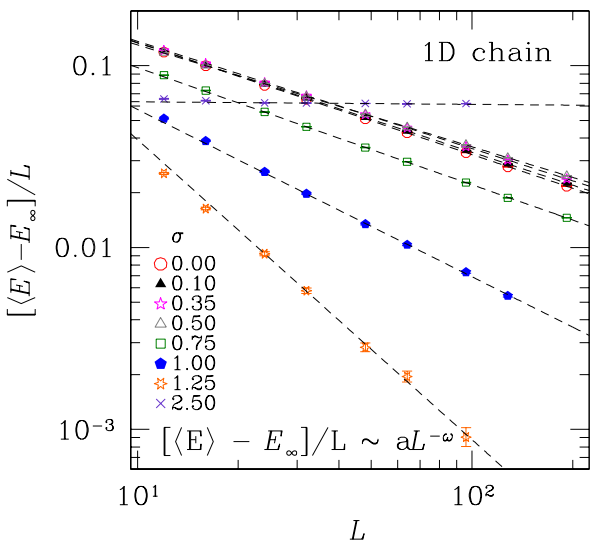

FIG. 10: (Color online) Mean $[\langle E\rangle - E_\infty]/L$ as a function of system size L for several values of σ. The data are expected to decay as a power of the system size with an exponent ω. Note that for the SK limit $\omega \approx 2/3$ at $T = 0$ in agreement with other predictions[8–10,41] [see Fig. 11 for $\omega(\sigma)$] and that for $\sigma = 2.5$ we obtain $\omega = 0$, i.e., a horizontal line.

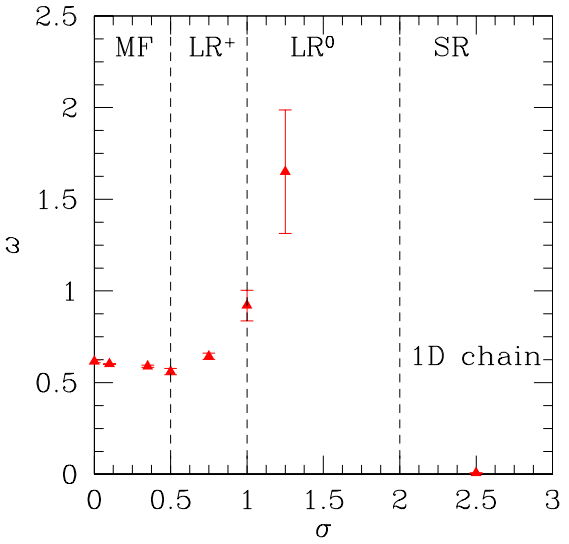

FIG. 11: (Color online) Exponent of the mean energy (ω) as a function of σ, according to Eq. (1). ω increases from the SK value ($\sim 2/3$) for increasing σ and then drastically drops to zero in the short-range phase (SR), i.e., the energy excess scales as $\sim 1/L$. The exponents are only estimated for the four largest system sizes studied for a given value of σ. See Tab. I for details. In this and following figures, the boundaries between the different universality classes are denoted by vertical dashed lines.

thus we will focus on comparing the present results to data for the SK model. In Fig. 10 we show data for all values of σ studied. For increasing σ, ω increases rapidly and then drops to zero in the SR phase, in agreement with our results on the ladder system (Sec III B). This behavior can be seen in details in Fig. 11 where we show the behavior of ω [see Eq. (1)], in detail for the different universality classes.

The behavior of the energy fluctuations is shown in Fig. 12 as a function of system size L for several values of σ. In the SK limit there are contradicting predictions regarding the power-law exponent ρ of the energy fluctuations σ_E. While Crisanti *et al.*[42] find $\rho = 5/6$, Bouchaud *et al.*[10] and Aspelmeier *et al.*[43] find $\rho = 3/4$. In this work we obtain $\rho = 0.775(2)$ ($Q = 0.58$; fits done for $L \geq 64$), which is also in agreement with the work by Palassini.[8] In Fig. 13 we show the σ-dependence of ρ. It is noteworthy that ρ decreases from the mean-field value $\sim 3/4$ to $1/2$ in the short-range universality class. This is to be expected as for $\sigma \to \infty$ the central limit theorem predicts that $\rho = 1/2$.[10] Note that again the results found agree with the prediction of the short-range ladder system in Sec. III B.

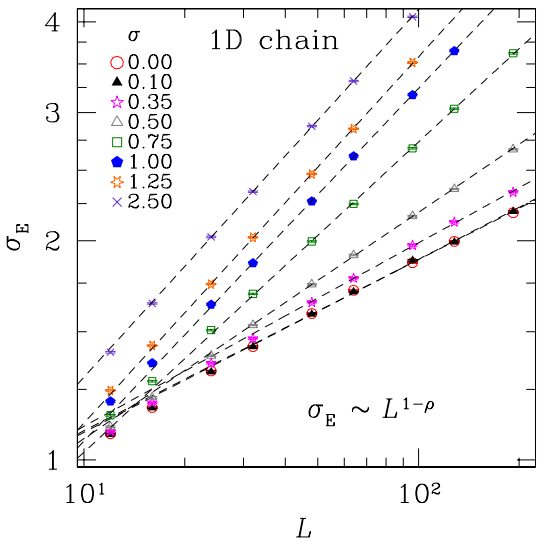

FIG. 12: (Color online) Standard deviation σ_E as a function of system size L for several values of σ. The data for σ_E/L are expected to decay as a power of the system size with an exponent ρ. Note that for the SK limit $\rho \approx 3/4$, in agreement with other predictions[8,10,43]. [See Fig. 13 for $\rho(\sigma)$].

D. Limiting Distribution

In order to further strengthen the conjecture that ground-state energy distributions remain skewed in the thermodynamic limit for the mean-field phase, in this

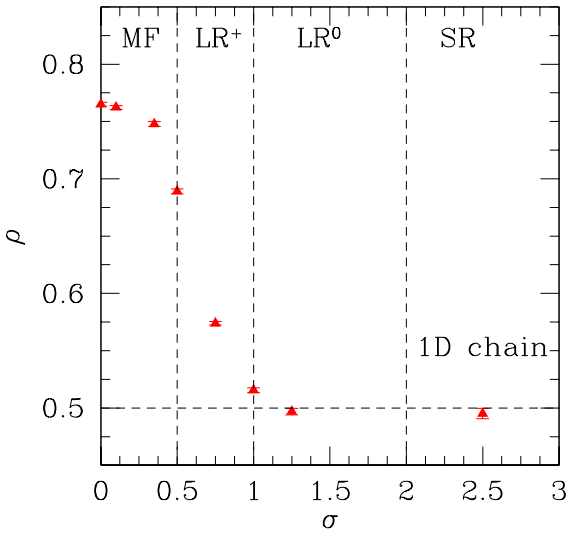

FIG. 13: (Color online) Exponent for the energy fluctuations ρ as a function of σ [see Eq. (2)]. For $\sigma \to 0$ $\rho \approx 3/4$ in agreement with Refs. 43, 10, and 8. For $\sigma \to \infty$, $\rho \to 1/2$, as predicted by the central limit theorem, and in agreement with the results on the ladder system presented in Sec. III B.

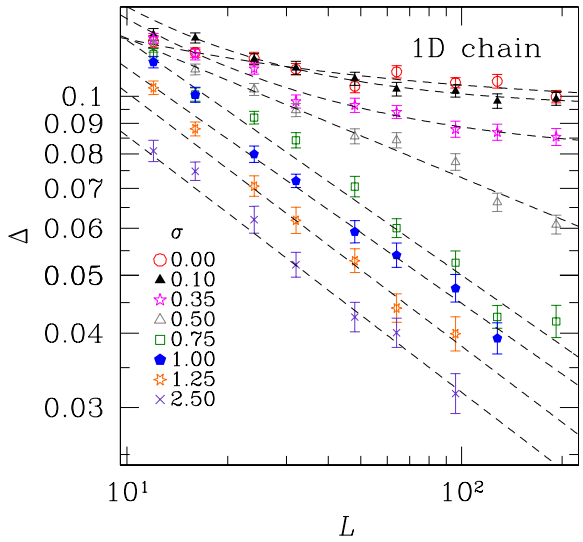

FIG. 14: (Color online) Difference in area between the actual data for the energy probability distributions of the one-dimensional Ising chain to a Gaussian limiting distribution as a function of system size L for several values of σ [see Eq. (19)]. In the MF phase ($\sigma < 0.5$) the area difference tends to a constant for increasing system size, whereas for $\sigma \geq 0.5$ the area difference decays with a power of the system size. Note the close resemblance to the behavior found for the skewness of the distribution, Fig. 9.

section we study the area deviation of the normalized energy distributions in comparison to a Normal distribution $N(\epsilon)$. We define the area difference Δ via

$$\Delta = \int_{\epsilon} |P(\epsilon) - N(\epsilon)| d\epsilon \, , \tag{19}$$

where $P(\epsilon)$ are the actual rescaled data [Eq. (5)]. In Fig. 14 we show the area difference as a function of system size L for several values of σ. The data for $\sigma < 0.5$ can be well fitted by a functional form $\sim f + g/L^h$, i.e., the area difference tends to a nonzero constant in the thermodynamic limit. This is not the case for $\sigma \geq 0.5$ where the area difference decays with a power-law of the system size, thus showing that the difference between the data and a Gaussian limiting distribution decreases for increasing L.

Palassini[8] has fitted the data for the scaled probability distribution functions of the SK model, Eq. (5), to a modified Gumbel distribution[1,3,19] $g_m(\epsilon)$, and finds good agreement between the data and the fit, especially when studying the cumulative distributions $Q(\epsilon) = \int^{\epsilon} P(x)dx$. In addition, Palassini shows that the best fit seems to be obtained for $m = 6$, although to date is unclear why the aforementioned value of m fits the data best. Because outside the MF universality class the limiting distribution function seem to converge to a Normal distribution, we modify the standard modified Gumbel distribution by taking into account a Normal contribution,[44] i.e.,

$$g'_m(\epsilon) = N(y) g_m(y) \tag{20}$$

where

$$y = \frac{\epsilon - \mu}{\nu} \tag{21}$$

and

$$g_m(\epsilon) = w_1 \exp\left[my - me^y\right] \tag{22}$$

is the modified Gumbel distribution and

$$N(\epsilon) = w_2 \exp\left[m_2 y^2\right] \tag{23}$$

is a Normal distribution. Here μ is the most-probable value, ν a standard deviation, and w_i represent an overall normalization factor. For simplicity, we can fix $m = 6$ and study the behavior of the coefficient m_2 as a function of system size for different values of σ. Note that for $m_2 = 0$ $g'_m(x) \propto g_m(x)$, up to a global scaling factor. A multiplicative ansatz [instead of for example an additive ansatz of the form $aN(\epsilon) + bg_m(\epsilon)$] can be motivated by keeping in mind that for short-range interactions, the system can be divided into subsystems which contribute almost independently to the total energy. In Fig. 15 we show data for m_2 vs L for a few representative values of σ. Our results show that for $\sigma = 0$ (SK model) m_2 converges to a value close to zero for $L \to \infty$. For $0 < \sigma \leq 0.5$ the limiting distribution is non-Gaussian, yet m_2 is small, but finite. For $\sigma > 0.5$ the Gaussian contribution via m_2 dominates in the thermodynamic limit,

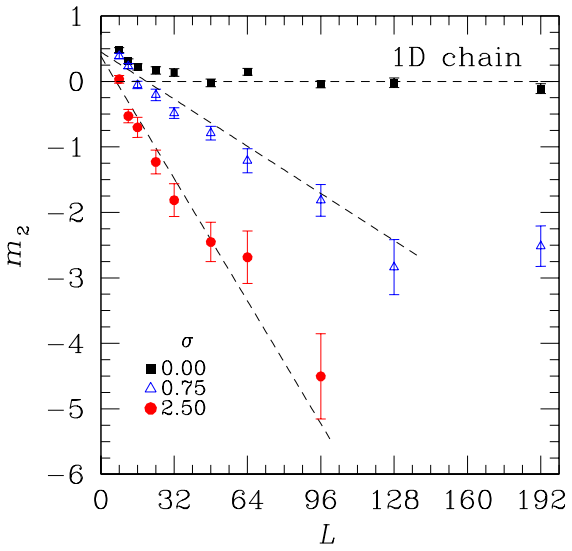

FIG. 15: (Color online) Coefficient m_2 to the quadratic correction term in the modified Gumbel distribution, Eq. (20), as a function of system size for several values of the power-law exponent σ. The data show that m_2 converges to a value close to zero for the SK model in the thermodynamic limit thus suggesting that the energy distributions of the SK model are possibly well described by a modified Gumbel distribution function in agreement with results from Ref. 8. For all $\sigma > 0$, m_2 tends to a finite negative value in the thermodynamic limit. For large values of σ, m_2 dominates thus showing that in the SR universality class the limiting probability distribution is well described by a Gaussian. The dashed lines are guides to the eye.

as can be seen in Fig. 15. This shows that the energy distributions in the SK model can be well described in the thermodynamic limit by a modified Gumbel distribution. In order to test the existence of small Gaussian corrections to the modified Gumbel distribution for the SK model, large-scale simulations probing the tails of the distribution function in detail would be required which are beyond the scope of this work. For all other values of $\sigma < 0.5$ there are clearly Gaussian corrections to the Gumbel distribution, whereas for $\sigma \geq 0.5$ the data in the thermodynamic limit are well described by a Normal limiting distribution. This could be due to the fact that there are no length-scales associated with the mean-field model. Thus any length-scale associated effects will scale with system size. This is not the case in the short-range models where a length scale will not necessarily scale with system size, therefore yielding a Normal distribution in the thermodynamic limit.

E. Finite Temperatures

We want to test if the fact that the ground-state energy distribution of the SK model is skewed in the thermodynamic limit is a unique property of the ground state, or if similar effects can be observed at finite temperatures. Because the parallel tempering Monte Carlo method used to compute the ground-state energies of the one-dimensional Ising chain at small values of σ requires the system to be simulated at several temperatures ranging to values well above the spin-glass transition (for the SK model $T_c = 1$), we have also studied the behavior of the internal energy distributions in the mean-field limit as a function of temperature. The internal energy U for a given disorder realization $\{J_{ij}\}$ is given by

$$U = \langle \mathcal{H}(\{J_{ij}\}, \{S_i\}) \rangle \ , \tag{24}$$

where the Hamiltonian $\mathcal{H}$ is given by Eq. (12). Here $\langle \cdots \rangle$ represents a thermal average over t_{eq} Monte Carlo steps that we perform after having equilibrated the system for a time t_{eq} (see Tab. I for details).

Figure 16 shows data for the skewness of the internal energy distributions as a function of system size for several temperatures ranging from the ground-state to well above the critical temperature. The results show that the skewness of the distributions tend to a constant value in the thermodynamic limit for $T \leq T_c$ (curved fitting functions in a log-log plot, Fig. 16), thus showing that skewed energy distributions seem to persist for any temperature below the critical temperature. For temperatures above the critical temperature, the skewness shows again a power-law behavior thus suggesting that for $T > T_c$ the limiting distribution is Normal, as one would expect. Therefore, the limiting probability distribution is skewed in the thermodynamic limit for all temperatures below the critical point.

The inset of Fig. 16 shows the skewness of the probability distribution function of the internal energy of the SK model for $L = 192$ as a function of temperature. The data show a peak around $T_c = 1$. We expect the functional form of the skewness to remain approximatively the same for $L \to \infty$ when $T < T_c$, whereas for $T > T_c$ we expect for the skewness $\zeta_E \to 0$ in the thermodynamic limit. It would be interesting to understand the origins of this behavior of the mean-field model analytically.

For nonzero values of σ we find finite-temperate results in agreement with the data presented in Sec. IV C: the distributions become Normal in the thermodynamic limit.

V. SUMMARY & CONCLUSIONS

We have studied in detail the probability distribution function of the ground-state energy of the one-dimensional Ising spin chain with random power-law interactions for several values of the power-law exponent

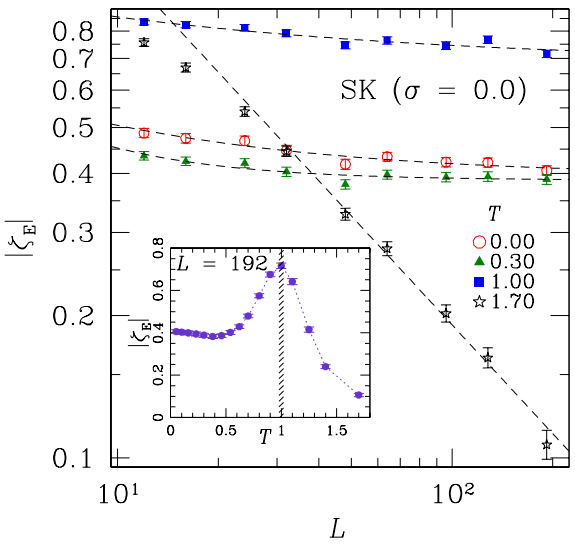

FIG. 16: (Color online) Skewness of the internal energy probability distribution functions of the SK model as a function of system size for different temperatures. The data show a curvature for $T \leq T_c$ in a log-log scale thus suggesting that the skewness converges to a constant value in the thermodynamic limit. For $T > T_c = 1$ the skewness decays with a power of the system size (Normal limiting probability distribution function). The inset shows the skewness of the internal energy distribution of the SK model for $L = 192$ (largest system size studied) as a function of temperature. The data show that for finite system sizes the skewness seems to peak at the transition ($T_c = 1$, shaded area).

σ. Using sophisticated parallel-tempering methods (fast for small values of σ) and a new branch, cut & price algorithm (fast for large values of σ), relatively large system sizes have been studied over the full range of the parameter σ.

For the SK limit, when $\sigma = 0$, our results agree with previous numerical work by Palassini.[8] We find by studying different moments of the distribution, that the SK model has a skewed probability distribution function in the thermodynamic limit that is well fitted by a modified Gumbel distribution, possible with small Gaussian corrections. This behavior is not only valid for the ground-state energy, but also for energies below the critical temperature.

By varying the power-law exponent σ we scan several universality classes and show that for the non-mean-field regime when $\sigma > 0.5$ the probability distribution functions converge to a Normal distribution in the thermodynamic limit, in agreement with a short-range spin-glass ladder. Thus a skewed probability distribution function is a characteristic property of the mean-field spin-glass model and the change of the distribution's characteristic coincides with the transition line between the MF and LR universality classes. This behavior again poses the question, of whether the mean-field description of spin glasses is adequate for non-mean-field models, as has been observed previously by studying other measurable quantities.[45–48]

Thus far it is unclear to us, why the limiting distribution for the SK case is well described by a modified Gumbel distribution with parameter $m > 1$, i.e., an extreme-value distribution for selecting the m'th smallest value out of a large number of M uncorrelated values.[1] If all 2^N energy levels of a system with N spin were uncorrelated, then the ground state would be simply the minimum of all 2^N uncorrelated values and a standard Gumbel distribution ($m = 1$) would be the limiting distribution. Clearly the energy values of a spin glass are not fully uncorrelated, but recently it has been observed[49] that the energy levels of the Edwards-Anderson model behave at least locally (i.e., in small intervals) like a random-energy model. This might be the underlying reason why a Gumbel distribution seems to describe the data best, as well as for the occurrence of a non-vanishing skewness in the MF case for $\sigma < 0.5$.

In general, we see that by studying the distributions of measurable quantities such as for the ground-state energy, we have another approach to discriminate mean-field type behavior from simpler structures of the phase space. Therefore this approach supplements other numerical means of studying the organization of phase space, such as calculating the distributions of overlaps,[50] clustering configurations,[51] or the calculation of correlation-matrix eigenvalues.[52] Hence, it should be fruitful to study the distributions of ground-state energies in detail also for other models. This is especially interesting when a disorder-driven phase transition occurs, such as for parameterized random bond models, random-field systems, or optimization algorithms on random graphs. So far the body of the ground-state energy distributions has been tested in detail. More information about the tails of the distributions could be accessed using rare-event techniques[44] also for the standard spin-glass models in finite and infinite dimensions.

APPENDIX A: PARALLEL TEMPERING GROUND-STATE SEARCH

In this Section we describe the different numerical tools to compute ground-state instances of the one-dimensional Ising chain fast. As introduced in Refs. 15 and 37 we use parallel tempering Monte Carlo[35,36] to calculate ground states. In Ref. 15 is has already been mentioned that parallel tempering Monte Carlo performs poorly for large values of σ. In particular, for $\sigma \geq 2.5$ we find that in practice the time to find a ground state scales exponentially[16] in the system size. In order to overcome this limitation we use the branch, cut & price algorithm described below.

For details regarding the parallel tempering approach see Refs. 35 and 36. Here we only discuss details that are

TABLE I: Parameters of the parallel tempering Monte Carlo simulations. The table shows the total number of Monte Carlo steps $t_{\rm eq}$ used for each value of σ and L. We use between 10 and 17 temperatures, depending on the system size, to ensure that the acceptance ratios of the parallel tempering moves are larger than ~ 0.30. The lowest temperature used is 0.05, the highest 1.70. For the internal energy distributions (Sec. IV E) we compute thermally averaged values of the internal energy for a given disorder realization after equilibrating for $t_{\rm eq}$ Monte Carlo steps. The averages are done over another period of $t_{\rm eq}$ Monte Carlo steps. For $\sigma = 2.50$ and $L = 96$ the calculations have been done using the BCP algorithm (Appendix B).

σ	$8, 12, 16$	$24, 32$	$48, 64$	$96, 128$	192
0.00	2×10^3	4×10^3	8×10^3	4×10^4	12×10^4
0.10	2×10^3	4×10^3	8×10^3	4×10^4	12×10^4
0.35	2×10^3	4×10^3	8×10^3	4×10^4	12×10^4
0.50	2×10^3	4×10^3	8×10^3	4×10^4	12×10^4
0.75	2×10^3	4×10^3	8×10^3	4×10^4	12×10^4
1.00	2×10^3	4×10^3	8×10^3	8×10^4	6×10^5
1.25	2×10^3	4×10^3	6×10^4	6×10^5	
2.50	2×10^3	4×10^3	2×10^5		

of importance to the ground-state calculations and give the parameters of the simulation in Table I. If we take the lowest temperature $T_{\rm min}$ to be 0.05 ($T_{\rm min} \ll T_{\rm c}$), then the minimum-energy state found at this temperature is with very high probability the ground state. To test whether the true ground state has been reached, four criteria have to be met: (i) the same minimum-energy state has to be reached from two independent replicas at $T_{\rm min}$ for all samples, and (ii) this state has to be reached during $t_{\rm eq}$ sweeps in both copies. (iii) We simulate for further $t_{\rm eq}$ sweeps to ensure that the energies found do not change, and (iv) the system has to obey the equilibration test for the one-dimensional Ising chain, introduced in Ref. 15. In this test the link overlap $q_{\rm l}$ has to equate the link overlap calculated from the internal energy $q_{\rm l}(U)$ via the relation

$$q_{\rm l} = 1 - \frac{2T|[U]_{\rm av}/L|}{(T_c^{\rm MF})^2} \ , \qquad \text{(A1)}$$

where $T_{\rm c}^{\rm MF}$ is given by Eq. (15), U is given by Eq. (24), and

$$q_l = \frac{2}{N} \sum_{i,j} \frac{[J_{ij}^2]_{\rm av}}{(T_c^{MF})^2} [\langle S_i S_j \rangle^2]_{\rm av} \ . \qquad \text{(A2)}$$

Once both sides of Eq. (A1) agree, the system is in equilibrium (see Fig. 17). Note that this is the case for the parameters listed in Table I. If any of the aforementioned criteria are not met (usually one instance in 10^5), the calculated ground-state instance is rejected.

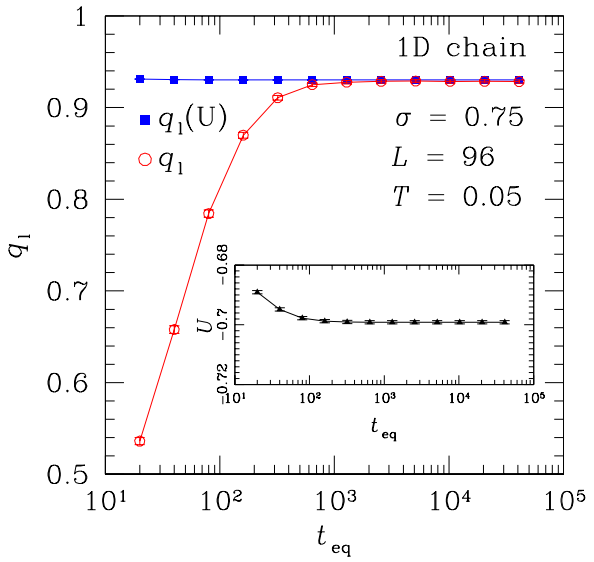

FIG. 17: (Color online) Equilibration plot for the one-dimensional Ising chain: Average link overlap as a function of Monte Carlo steps $t_{\rm eq}$ calculated directly [Eq. (A2)], and via the internal energy [Eq. (A1)] averaged over the last half of the sweeps for $L = 96$, $T = 0.05$, and $\sigma = 0.75$. The data are equilibrated for $t_{\rm eq} \approx 10^4$ MCS, in the simulations 4×10^4 MCS have been used. Data for 2500 disorder realizations.

APPENDIX B: BRANCH, CUT & PRICE ALGORITHM

In this section we briefly explain how exact ground states of one-dimensional Ising spin-glass instances can be computed fast for large values of σ. To this end, we extend the branch-and-cut approach to a branch, cut & price (BCP) method originating in combinatorial optimization. Since this approach has not yet been applied for spin glasses, we give more details in the following subsection and discuss the performance in a subsequent section. Again, for the fundamentals of the applied algorithm, i.e., the standard branch & cut approach, we refer the reader to Refs. 38 and 39.

1. Algorithm

The problem of determining a ground state of an Ising spin glass instance is equivalent to determining a *maximum cut* in the interaction graph associated with the system.[38] In the maximum cut problem we are given a graph $G = (V, E)$ with nodes V and edges E. The nodes correspond to the spin sites, the edges to the bonds. Weights $c_{ij} \in \mathbb{R}$ are given for all edges $ij \in E$. Let $W \subset V$ be a subset of nodes. The *cut* $\delta(W)$ is defined as the set of edges having exactly one endpoint in W. The weight of a cut $\delta(W)$ is the sum of the weights of the edges in the cut, and the maximum cut problem is

to find a cut $\delta(W)$ of G with maximum weight among all possible node sets W. Determining a ground state of a spin-glass instance amounts to calculating a maximum cut in the interaction graph of the system, with edge weights chosen as $c_{ij} = -J_{ij}$ for $ij \in E$.

The maximum cut problem is NP-hard which makes it unlikely that there exists a solution algorithm running in a number of steps bounded by a polynomial in the size of the input. In practice, maximum cuts of reasonably sized instances can be determined exactly by using the branch-and-cut method from combinatorial optimization that has exponential worst-case running time. For an instance, we always maintain an upper and a lower bound for the optimum solution value of the maximum cut. Iteratively we improve upper and lower bounds until they are tight enough for proving optimality of a known solution. In the upper bound computations, a sequence of *linear programs* is solved. Solving a linear problem amounts to optimizing a linear objective function subject to a set of linear constraints. Details are explained in Refs. 38 and 39.

For an instance of the one-dimensional Ising chain with $L = 100$ spins and $\sigma = 3.0$, the default version of the branch-and-cut algorithm needs roughly 3h CPU time on average on a 1400 MHz Athlon processor. By extending the branch-and-cut algorithm to a *branch, cut & price* algorithm we achieve a better performance. Details about pricing algorithms can be found in Ref. 40.

The underlying idea of a pricing algorithm is as follows. There exists a variable for each edge $ij \in E$, and we use the terms edge and variable interchangeably. In the pure branch-and-cut algorithm we always work on the complete set of variables. However, in the extended algorithm we start doing branch-and-cut, but only work on a small fraction of all variables. We add necessary variables (and delete unnecessary ones) dynamically during the optimization process. This is done in the so-called *pricing* routine.

For the one-dimensional Ising chain, we make the assumption that for big enough values of the parameter σ the "long-range couplings" between two spins "far apart" from each other in the chain do not strongly affect the ground state and can be neglected temporarily. Thus, we start working on a graph $G = (V, E)$ consisting of all nodes but only of a fraction of all edges. In our tests it performed best when the input graph consisted of the $k\%$ edges with highest weights, measured in absolute value, where the parameter k is suitably chosen in order to minimize the total running time. (For example, for $\sigma = 3.0$ $k = 20$ is a good choice, for smaller σ the value of k is increased.) At well-defined steps in the algorithm the pricing routine checks whether there exists a (yet neglected) variable that has to be included in the variable set for maintaining correctness. If no variable is added, and upper and lower bounds are tight enough, we can prove optimality, and stop. For our model, we can further improve the quality of the upper bound within the BCP algorithm by separating not only the cycle inequalities[38] but also separating heuristically the so-called parachute inequalities[53] resulting in an improved bound and an additional speedup.

When the BCP algorithm is used, solving systems for $\sigma = 3.0$ takes on average 426 ± 55 seconds for $L = 100$ on the same 1400MHz Athlon processor that needed three hours on average for solving the same systems by branch-and-cut. In Ref. 15 it is reported that parallel tempering is less efficient in finding the ground state for bigger values of σ. Then parallel tempering needs longer to relax an inconvenient configuration. With the exact algorithm, in contrast, we expect pricing to be only effective for bigger σ. In this case we expect a speedup by using sparse graph techniques as explained above. For small σ instead, the system is of long-range type, and in the worst-case all neglected edges would have to be added in the pricing routine.

In the following section we experimentally determine the running time dependence of the BCP algorithm and its dependence on the parameter σ and on the system size.

2. Performance of the Algorithm

In this section we study the performance of the BCP algorithm for the one-dimensional Ising chain model. We compute ground states of samples for different system sizes L and values of the parameter σ. The studied ranges are $\sigma \in \{1.0, 1.5, 2.0, 2.5, 3.0\}$, and $L \leq 96$. We compute between 1000 and 6000 samples per size and σ-value for small- and medium-sized instances and at least 100 samples for the largest instances. All runs are performed on a Linux cluster of identical AMD Athlon 1800+ machines. Instances of size $L \leq 48$ and $\sigma \geq 2.0$ are solved within seconds; for $\sigma = 3.0$, computing a ground state of $L = 280$ spins takes on average 5161 ± 275 seconds. The hardest instances, $L = 96, \sigma = 1.5$ needs up to a day computing time on one processor.

As argued before in Ref. 54, there is no easy and "ideal" performance measure for a branch-and-cut algorithm. This remains true for its extension to the BCP algorithm. As a measure of the performance of the latter, we could use the needed CPU time which however is machine dependent, or the number of solved linear programs (lps), see Refs. 55 and 54. For $\sigma \lesssim 2$ we find that the number of lps n_{lps} is strongly and almost linearly correlated with the CPU time t_{CPU}, see Fig. 18. The same is true for the pure branch-and-cut algorithm. However, for $\sigma \gtrsim 2.0$ the CPU time for solving an lp considerably varies between different samples of the same size, as can be seen for $L = 64$ and $\sigma = 3.0$ in the scatter plot, Fig. 18.

A reason for this behavior is the following: In order to keep the program flexible, in each iteration we both add new constraints to the current linear program and remove constraints that once have been added but have turned out to be unimportant. (Re-)Optimizing an lp is very

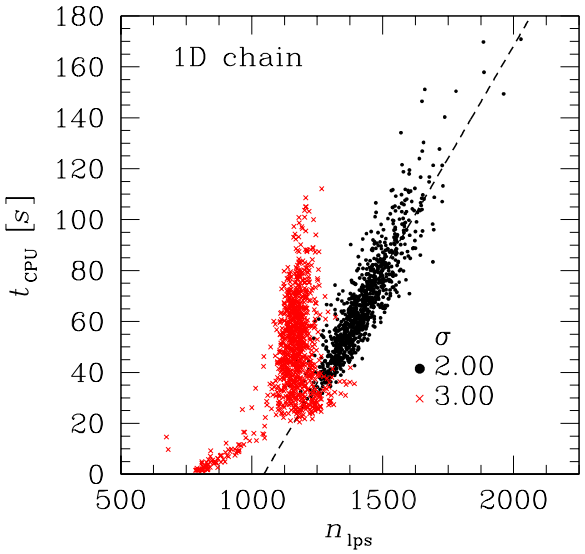

FIG. 18: (Color online) Scatter plot for the CPU time $t_{\rm CPU}$ in seconds versus the number of lps $n_{\rm lps}$ for 1000 randomly chosen samples with $L = 64$. The data for $\sigma = 2.0$ (black dots) are strongly correlated. The dashed line is a guide to the eye. In contrast, data for $\sigma = 3.0$ (red crosses) show strong sample-to-sample variations.

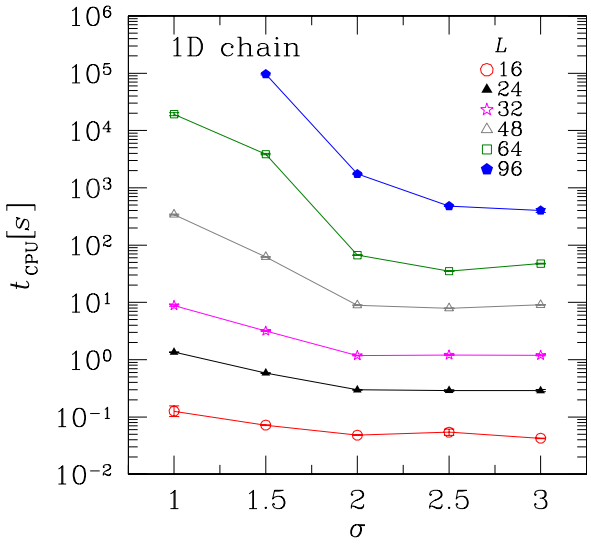

FIG. 19: (Color online) Mean CPU time $t_{\rm CPU}$ in seconds for determining a ground state versus σ for different L in a linear-log scale. For increasing σ and for all system sizes L the time to find a ground-state configuration decreases thus showing that the algorithm becomes more efficient when the interactions are more short-ranged ($\sigma \to \infty$).

fast if only a small number of constraints changes from one iteration to the next but takes considerably longer if a substantial change occurs. In the pricing extension, we start working on a subset of the variables and might add further variables as explained above. Possibly a "bad" subset of variables is chosen, in the sense that many of the added constraints become unimportant later and are removed again. Then the lps change considerably and their solution takes long. This is more probable for big σ, as we start working on a small subset of the variables. For smaller values of σ instead, we start working on a bigger fraction of all variables and find a stronger correlation between number of lps and CPU time.[56] Given the broad variation in the CPU time per lp for some values of σ, we use the mean of the CPU time as performance measure. We notice that the figures remain qualitatively comparable when the mean of the linear programs is taken instead of the CPU time. We have checked that the mean of both the CPU time and the number of linear programs is defined for our sampling as the distribution shows a pronounced tail. Performing a detailed statistical analysis we show that the data are thin-tail distributed[1] with a well-defined mean.

In Fig. 19 we show the average CPU time for solving an instance as a function of σ, for different system sizes L. Ground states are computed fast for big values of the parameter σ, whereas it takes considerably longer for smaller $\sigma \leq 1.5$. This effect becomes more apparent with increasing system size L.

We also study the CPU time as a function of the total number of edges, i.e., the total number of variables, for different values of σ. The increase in the CPU time with the number of variables is consistent with a polynomial dependency, even for the smallest studied value of σ. When fitting a function of the form $f(m) \sim am^b$, with m being the number of variables (bonds), we obtain $a = 0.009 \pm 0.007$, $b = 1.3 \pm 0.1$ for $\sigma = 2.0$. A similar behavior can be found when studying the CPU time as a function of system size L, see Fig. 20.

A qualitatively similar behavior can be found in the data when plotted as a function of lps instead of CPU time (not shown).

ACKNOWLEDGMENTS

We would like to thank I. A. Campbell, P. C. Holdsworth, O. Martin, S. Trebst, M. Troyer, D. Würtz, and A. P. Young for discussions. A.K.H. obtained financial support from the *VolkswagenStiftung* (Germany) within the program "Nachwuchsgruppen an Universitäten". F.L. has been supported by the German Science Foundation (DFG) in the project Ju 204/9-1. The calculations were performed on the Asgard cluster at ETH Zürich and on the SCALE cluster of E. Speckenmeyer's group in Cologne. We are indebted to M. Troyer and G. Sigut for allowing us to use the idle time on the Asgard cluster.

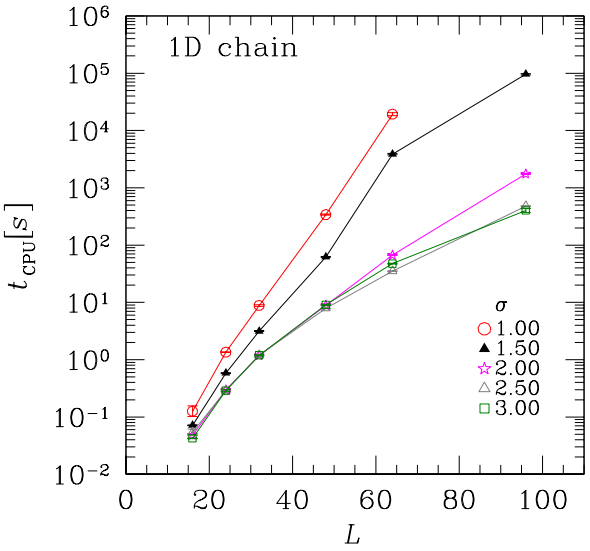

FIG. 20: (Color online) Mean CPU time for determining a ground state versus the system size L for different values of σ in a linear-log scale. Note that the CPU time increases slower than exponential for all values of σ studied. For $\sigma \geq 2.5$ the CPU time increases with a power of the system size.

[1] E. J. Gumbel, *Large deviations techniques in decision, simulation, and estimation* (John Wiley and Sons, New York, 1958).

[2] S. Hergarten, *Self-Organized Criticality in Earth Systems* (Springer-Verlag, Berlin, 2002).

[3] S. T. Bramwell, J.-Y. Fortin, P. C. Holdsworth, S. Peysson, J.-F. Pinton, B. Portelli, and M. Sellitto, *Magnetic fluctuations in the classical XY model: The origin of an exponential tail in a complex system*, Phys. Rev. E **63**, 041106 (2001).

[4] R. N. Mantegna and H. E. Stanley, *Introduction to Econophysics* (Cambridge University Press, Cambridge, 1999).

[5] J. M. Kim, M. A. Moore, and A. J. Bray, *Zero-temperature directed polymers in a random potential*, Phys. Rev. A **44**, 2345 (1991).

[6] T. Halpin-Healy, *Directed polymers in random media: Probability distributions*, Phys. Rev. A **44**, R3415 (1991).

[7] R. Albert and A.-L. Barabási, *Statistical mechanics of complex networks*, Rev. Mod. Phys. **74**, 47 (2002).

[8] M. Palassini, *Ground-state energy fluctuations in the Sherrington-Kirkpatrick model* (2003), (cond-mat/0307713).

[9] A. Andreanov, F. Barbieri, and O. C. Martin, *Large deviations in spin-glass ground-state energies*, European Physical Journal B **41**, 365 (2004).

[10] J.-P. Bouchaud, F. Krzakala, and O. C. Martin, *Energy exponents and corrections to scaling in Ising spin glasses*, Phys. Rev. B **68**, 224404 (2003).

[11] K. Binder and A. P. Young, *Spin glasses: Experimental facts, theoretical concepts and open questions*, Rev. Mod. Phys. **58**, 801 (1986).

[12] A. J. Bray, M. A. Moore, and A. P. Young, *Lower critical dimension of metallic vector spin-glasses*, Phys. Rev. Lett **56**, 2641 (1986).

[13] D. S. Fisher and D. A. Huse, *Equilibrium behavior of the spin-glass ordered phase*, Phys. Rev. B **38**, 386 (1988).

[14] L. Leuzzi, *Critical behaviour and ultrametricity of ising spin-glass with long-range interactions*, J. Phys. A **32**, 1417 (1999).

[15] H. G. Katzgraber and A. P. Young, *Monte Carlo studies of the one-dimensional Ising spin glass with power-law interactions*, Phys. Rev. B **67**, 134410 (2003).

[16] H. G. Katzgraber and A. P. Young, *Geometry of large-scale low-energy excitations in the one-dimensional Ising spin glass with power-law interactions*, Phys. Rev. B **68**, 224408 (2003).

[17] M. Mézard, G. Parisi, and M. A. Virasoro, *Spin Glass Theory and Beyond* (World Scientific, Singapore, 1987).

[18] J. Bouchaud and M. Mézard, *Universality classes for extreme-value statistics* , J. Phys. A **30**, 7997 (1997).

[19] B. Portelli, P. C. W. Holdsworth, M. Sellitto, and S. T. Bramwell, *Universal magnetic fluctuations with a field-induced length scale*, Phys. Rev. E **64**, 036111 (2001).

[20] A. K. Hartmann and H. Rieger, *Optimization Algorithms in Physics* (Wiley-VCH, Berlin, 2001).

[21] A. K. Hartmann and H. Rieger, *New Optimization Algorithms in Physics* (Wiley-VCH, Berlin, 2004).

[22] W. H. Press, S. A. Teukolsky, W. T. Vetterling, and B. P. Flannery, *Numerical Recipes in C* (Cambridge University Press, Cambridge, 1995).

[23] I. Morgenstern and K. Binder, *Magnetic correlations in two-dimensional spin-glasses*, Phys. Rev. B **22**, 288 (1980).

[24] Y. Ozeki, *Ground State Properties of the ±J Ising Model in Two Dimensions*, J. Phys. Soc. Jpn. **59**, 3531 (1990).

[25] D. Sherrington and S. Kirkpatrick, *Solvable model of a spin glass*, Phys. Rev. Lett. **35**, 1792 (1975).

[26] Note that the distance r_{ij} between two spins i and j on the chain is determined by $r_{ij} = 2R\sin(\alpha/2)$, where R is the radius of the chain and α is the angle between the two sites on the circle. The previous expression can be rewritten in terms of the system size L and the positions of the spins to obtain $r_{ij} = (L/\pi)\sin(\pi|i-j|/L)$.

[27] The stiffness exponent θ defines the energy scale required to excite a domain wall in a spin system. Usually it is defined via the change in energy after inducing a domain wall trough a change in boundary conditions, i.e., $\Delta E = [|E_{\rm p} - E_{\rm ap}|]_{\rm av} \sim L^{\theta}$ with $E_{\rm p}$ the ground-state energy of the system with periodic, and $E_{\rm ap}$ the ground-state energy of the system with antiperiodic boundary conditions. When $\theta < 0$ the system is unstable towards excitation, therefore $T_{\rm c} = 0$.

[28] A. J. Bray and M. A. Moore, *Lower critical dimension of Ising spin glasses: a numerical study*, J. Phys. C **17**, L463 (1984).

[29] W. L. McMillan, *Domain-wall renormalization-group study of the three-dimensional random Ising model*, Phys. Rev. B **30**, R476 (1984).

[30] W. L. McMillan, *Domain-wall renormalization-group study of the two-dimensional random Ising model*, Phys. Rev. B **29**, 4026 (1984).

[31] N. Kawashima and A. P. Young, *Phase transition in the three-dimensional ±J Ising spin glass*, Phys. Rev. B **53**, R484 (1996).

[32] A. K. Hartmann, *Scaling of stiffness energy for three-dimensional ±J Ising spin glasses*, Phys. Rev. E **59**, 84 (1999).

[33] H. G. Ballesteros, A. Cruz, L. A. Fernandez, V. Martin-Mayor, J. Pech, J. J. Ruiz-Lorenzo, A. Tarancon, P. Tellez, C. L. Ullod, and C. Ungil, *Critical behavior of the three-dimensional Ising spin glass*, Phys. Rev. B **62**, 14237 (2000).

[34] A. K. Hartmann and A. P. Young, *Lower critical dimension of Ising spin glasses*, Phys. Rev. B **64**, 180404(R) (2001).

[35] K. Hukushima and K. Nemoto, *Exchange Monte Carlo method and application to spin glass simulations*, J. Phys. Soc. Jpn. **65**, 1604 (1996).

[36] E. Marinari, G. Parisi, J. J. Ruiz-Lorenzo, and F. Ritort, *Numerical evidence for spontaneously broken replica symmetry in 3d spin glasses*, Phys. Rev. Lett. **76**, 843 (1996).

[37] J. J. Moreno, H. G. Katzgraber, and A. K. Hartmann, *Finding low-temperature states with parallel tempering, simulated annealing and simple Monte Carlo*, Int. J. Mod. Phys. C **14**, 285 (2003).

[38] F. Barahona, M. Grötschel, M. Jünger, and G. Reinelt, *An application of combinatorial optimization to statistical physics and circuit layout design models*, Operations Research **36**, 493 (1988).

[39] F. Liers, M. Jünger, G. Reinelt, and G. Rinaldi, in *New Optimization Algorithms in Physics*, edited by A. K. Hartmann and H. Rieger (Wiley-VCH, Berlin, 2004).

[40] M. Jünger, G. Reinelt, and S. Thienel, in *DIMACS Series in Discrete Mathematics and Theoretical Computer Science*, edited by W. Cook, L. Lovasz, and P. Seymour (American Mathematical Society, 1995), vol. 20.

[41] S. Boettcher, *Numerical results for ground states of spin glasses on Bethe lattices*, Eur. Phys. J. B **31**, 29 (2003).

[42] A. Crisanti, G. Paladin, and H.-J. S. A. Vulpiani, *Replica trick and fluctuations in disordered systems*, Journal de Physique I **2**, 1325 (1992).

[43] T. Aspelmeier, M. A. Moore, and A. P. Young, *Interface energies in Ising spin glasses*, Phys. Rev. Lett. **90**, 127202 (2002).

[44] A. K. Hartmann, *Sampling rare events: Statistics of local sequence alignments*, Phys. Rev. E **65**, 056102 (2002).

[45] M. Palassini and A. P. Young, *Triviality of the ground state structure in Ising spin glasses*, Phys. Rev. Lett. **83**, 5126 (1999).

[46] F. Krzakala and O. C. Martin, *Spin and link overlaps in 3-dimensional spin glasses*, Phys. Rev. Lett. **85**, 3013 (2000).

[47] H. G. Katzgraber, M. Palassini, and A. P. Young, *Monte Carlo simulations of spin glasses at low temperatures*, Phys. Rev. B **63**, 184422 (2001).

[48] A. P. Young and H. G. Katzgraber, *Absence of an Almeida-Thouless line in Three-Dimensional Spin Glasses*, Phys. Rev. Lett. **93**, 207203 (2004).

[49] H. Bauke and S. Mertens, *Universality in the level statistics of disordered systems*, Phys. Rev. E **70**, 025120(R) (2004).

[50] R. N. Bhatt and A. P. Young, *Search for a transition in the three-dimensional ±J Ising spin-glass*, Phys. Rev. Lett. **54**, 924 (1985).

[51] W. Barthel and A. K. Hartmann, *Clustering analysis of the ground-state structure of the vertex-cover problem*, Phys. Rev. E **70**, 066120 (2004).

[52] J. Sinova, G. Canright, and A. MacDonald, *Nature of Ergodicity Breaking in Ising Spin Glasses as Revealed by Correlation Function Spectral Properties*, Phys. Rev. Lett. **85**, 2609 (2000).

[53] M. Deza and M. Laurent, *Geometry of Cuts and Metrics, (Algorithms and Combinatorics Vol. 15)* (Springer-Verlag, New York, 1997).

[54] F. Liers, M. Palassini, A. K. Hartmann, and M. Jünger, *Ground state of the Bethe lattice spin glass and running time of an exact optimization algorithm*, Phys. Rev. B **68**, 094406 (2003).

[55] M. Palassini, F. Liers, M. Jünger, and A. P. Young, *Low-energy excitations in spin glasses from exact ground states*, Phys. Rev. B **68**, 064413 (2003).

[56] Another possibility for the broad distribution of the running time per lp could be a strong variation in the number of added and deleted variables. However, in our sampling this was not the case.